



Philosophical Magazine Letters

ISSN: (Print) (Online) Journal homepage: www.tandfonline.com/journals/tphl20

Sulphuric precipitates in novel titanium-based, sulphur-bearing bulk metallic glass – a BMG composite?

Bastian Adam, Alexander Kuball, Lucas Matthias Ruschel, Nico Neuber, Maximillian Frey & Ralf Busch

To cite this article: Bastian Adam, Alexander Kuball, Lucas Matthias Ruschel, Nico Neuber, Maximillian Frey & Ralf Busch (2024) Sulphuric precipitates in novel titanium-based, sulphur-bearing bulk metallic glass – a BMG composite?, *Philosophical Magazine Letters*, 104:1, 2376614, DOI: [10.1080/09500839.2024.2376614](https://doi.org/10.1080/09500839.2024.2376614)

To link to this article: <https://doi.org/10.1080/09500839.2024.2376614>



© 2024 The Author(s). Published by Informa UK Limited, trading as Taylor & Francis Group



Published online: 15 Jul 2024.



Submit your article to this journal [↗](#)



View related articles [↗](#)



View Crossmark data [↗](#)

Sulphuric precipitates in novel titanium-based, sulphur-bearing bulk metallic glass – a BMG composite?

Bastian Adam ^a, Alexander Kuball^b, Lucas Matthias Ruschel ^a,
Nico Neuber ^a, Maximilian Frey ^a and Ralf Busch ^a

^aChair of Metallic Materials (LMW), University of Saarland, Saarbrücken, Germany; ^bAmorphous Metal Solutions GmbH, Homburg, Germany

ABSTRACT

New titanium-based metallic glasses containing sulphur as a key element have recently been developed and are the subject of ongoing research related to the effects of sulphur introduction into glass-forming alloy systems. Here we report on the formation of sulphuric precipitates during solidification of a $\text{Ti}_{40}\text{Zr}_{35}\text{Cu}_{17}\text{S}_8$ alloy and on the occurrence of secondary intermetallic compound crystallization starting in sulphur-depleted zones around the precipitates. The alloy is a promising metallic glass for use as a structural and biomedical material as it shows a high yield strength and good corrosion resistance paired with a low density. The role of sulphur for the glass formation in the Ti-Zr-Cu-S system is discussed and specimens quenched into different structural states are investigated by means of high-energy synchrotron diffraction and electron microscopy. The electron microscopic findings reveal that sulphuric precipitates precede the crystallization of an intermetallic (Ti, Zr)₂Cu phase, which is the primary phase when sulphur is not present in the system and thus lead to a higher glass-forming ability. The sulphuric precipitates are found in specimens of various casting thickness and differ in their volume percentages depending on the size of the cast sample, while the secondary phase (Ti, Zr)₂Cu crystallizes heterogeneously in the interfaces between the sulphuric precipitates and the local matrix.

ARTICLE HISTORY



Received 15 November 2023
Accepted 12 June 2024

KEYWORDS

BMG; primary phase;
sulphuric precipitates;
metallic glasses;
crystallisation

1. Introduction

Bulk metallic glasses (BMG) have emerged as a group of promising new materials, featuring unique mechanical properties for engineering applications in terms of high yield strengths and exceptional elastic limits of about 2% strain [1]. Hence there is special interest in developing inexpensive and

CONTACT Bastian Adam  bastian.adam@uni-saarland.de  Chair of Metallic Materials (LMW), University of Saarland, Campus C6.3, 66123 Saarbrücken, Germany

© 2024 The Author(s). Published by Informa UK Limited, trading as Taylor & Francis Group
This is an Open Access article distributed under the terms of the Creative Commons Attribution License (<http://creativecommons.org/licenses/by/4.0/>), which permits unrestricted use, distribution, and reproduction in any medium, provided the original work is properly cited. The terms on which this article has been published allow the posting of the Accepted Manuscript in a repository by the author(s) or with their consent.

better glass-forming alloys for potential industrial applications [2]. To improve the glass-forming ability (GFA) and increase the resistance of BMGs against higher impurity content is the declared goal of many investigations in the sector of alloy development [3]. BMGs featuring sulphur as a key element were introduced by Kuball et al. in 2017 [4] and further investigated in our group's consecutive works [5–8]. With sulphur addition, the GFA increases by one order of magnitude for $\text{Ti}_{40}\text{Zr}_{35}\text{Cu}_{17}\text{S}_8$ as it rises from below 200 μm to 3 mm for ternary Ti-Zr-Cu alloys with the addition of sulphur [9,10]. As a structural engineering material $\text{Ti}_{40}\text{Zr}_{35}\text{Cu}_{17}\text{S}_8$ is particularly interesting, since it features attractive mechanical properties in combination with a high corrosion resistance and a decent critical casting thickness [10]. This can be achieved even when the alloy is synthesized from industrial-grade alloy Zr_{702} and cp-grade 2 Ti. These advantageous properties have led to increased research and prompted interest in the alloy's crystallization behaviour.

On the matter of primary crystallization phases, Kuball [5] and Bochtler [11] reported possible titanium sulphides and zirconium sulphides being present upon slow cooling from the equilibrium melt, which were observed during in-situ synchrotron experiments utilizing an electrostatic-levitation environment [12]. In the present work, samples with a thickness below the GFA of the $\text{Ti}_{40}\text{Zr}_{35}\text{Cu}_{17}\text{S}_8$ alloy as well as above the GFA were cast to probe different crystalline states of the system in depth using high-energy-synchrotron diffraction (HE-XRD), scanning electron microscopy (SEM) and transmission electron microscopy (TEM).

2. Materials and methods

The master alloy $\text{Ti}_{40}\text{Zr}_{35}\text{Cu}_{17}\text{S}_8$ was arc-melted from high-purity (99.99 wt%) Zr, Ti and commercial Cu_2S pre-alloy as previously described in reference [10]. The suction cast plates had a width of 12 mm and a length of 45 mm with thicknesses of 1, 1.5 and 2 mm, respectively.

Scanning electron microscopy was performed with a FEI Helios NanoLab600. The lamella for TEM investigation was prepared by Focused Ion Beam (FIB) machining with Ga-ions from the 1.5 mm thick plate as it showed a minor Bragg peak and therefore a high chance of finding the primary crystallization product in this casting thickness. The lamella was investigated with a JEOL Type JEM2011 TEM at an acceleration voltage of 200 kV.

The HE-XRD experiments were performed at the German Electron Synchrotron in Hamburg (DESY) at the PETRA III facility, in the department of the Swedish Material Science's Beamline P21.2. An X-ray radiation energy of 70 keV and a Varex 2D flat panel detector (XRD4343 CT) with 150 μm pixel size were utilized. Data correction and calculation of structure factor $S(Q)$ were performed with the PDFgetX3 software [13].

3. Results

High-energy synchrotron diffraction results are depicted in [Figure 1a](#). The overview shows the diffracted intensity for three different plate thicknesses of the $\text{Ti}_{40}\text{Zr}_{35}\text{Cu}_{17}\text{S}_8$ alloy. The synchrotron diffraction spectrum of the 1 mm plate indicates an X-ray amorphous structure with no presence of crystalline Bragg peaks. The 1.5 mm plate contains a minor crystalline fraction and the corresponding cooling rate is located closely to the critical cooling rate for obtaining fully amorphous plate samples. A larger presence of crystals can easily be determined in the 2 mm plate by the presence of sharp Bragg peaks making a significant contribution to the spectrum. The crystalline phase was assigned to a tetragonal $(\text{Ti}, \text{Zr})_2\text{Cu}$ crystal structure (I4/mmm) in accordance with the previously reported phase of that system [8,10]. The tetragonal $(\text{Zr}, \text{Ti})_2\text{Cu}$ phase (mp – 1215181) [15] resulted in the highest figure of merit during a search-match operation. This is a proportionally mixed crystal structure of Ti_2Cu and Zr_2Cu intermetallic phase [14]. The structure was further refined and separated from the amorphous background by a Rietveld refinement with statistical values of chi-square test χ^2 of 1.9 and a weighted residual R_{wp} of 3.3 with a goodness of fit (GOF) of 1.44, that was reached in the final refinement cycle.

While the synchrotron X-ray diffraction depicts a completely X-ray amorphous sample for the 1 mm thick plate of $\text{Ti}_{40}\text{Zr}_{35}\text{Cu}_{17}\text{S}_8$, on closer inspection with the SEM in back-scattering electron (BSE) imaging mode, a small amount of precipitates can be spotted as shown in [Figure 1a](#). These sulphuric precipitates seem to be omnipresent in all the investigated castings of $\text{Ti}_{40}\text{Zr}_{35}\text{Cu}_{17}\text{S}_8$ and appear throughout a variety of different casting thicknesses with varying volume proportions. A magnified backscattering electron image of the small sulphuric precipitate in the centre of the 1.5 mm plate specimen is shown in [Figure 2a](#), where a distinct difference in Z-contrast between matrix and the precipitate can be observed. The region between the amorphous matrix and the precipitate appears to be irregular in shape. The interphase between the sulphuric precipitate and the local matrix contains circular crystallites of a secondary crystalline phase with diameters reaching up to about 500 nm.

To investigate further, the 1.5 mm thick plate containing 1.1 A% (area percentage) of sulphides and also possessing small Bragg peaks belonging to $(\text{Ti}, \text{Zr})_2\text{Cu}$ crystallites in the synchrotron HE-XRD spectrum, was chosen for further analysis by transmission electron microscopy. The FIB cut through a sulphuric precipitate ([Figure 2b](#)) to observe three suspected phases provides a cross-section of the phases: the local matrix phase (A), the sulphuric precipitate (B) and the anticipated secondary crystal of the $(\text{Ti}, \text{Zr})_2\text{Cu}$ phase (C).

An interesting part of the lamella can be seen in the magnification of the FIB cut lamella in [Figure 2b](#), where the three phases are separated from each other. The particle looks like a starfish when split in half by the metallographic cut,

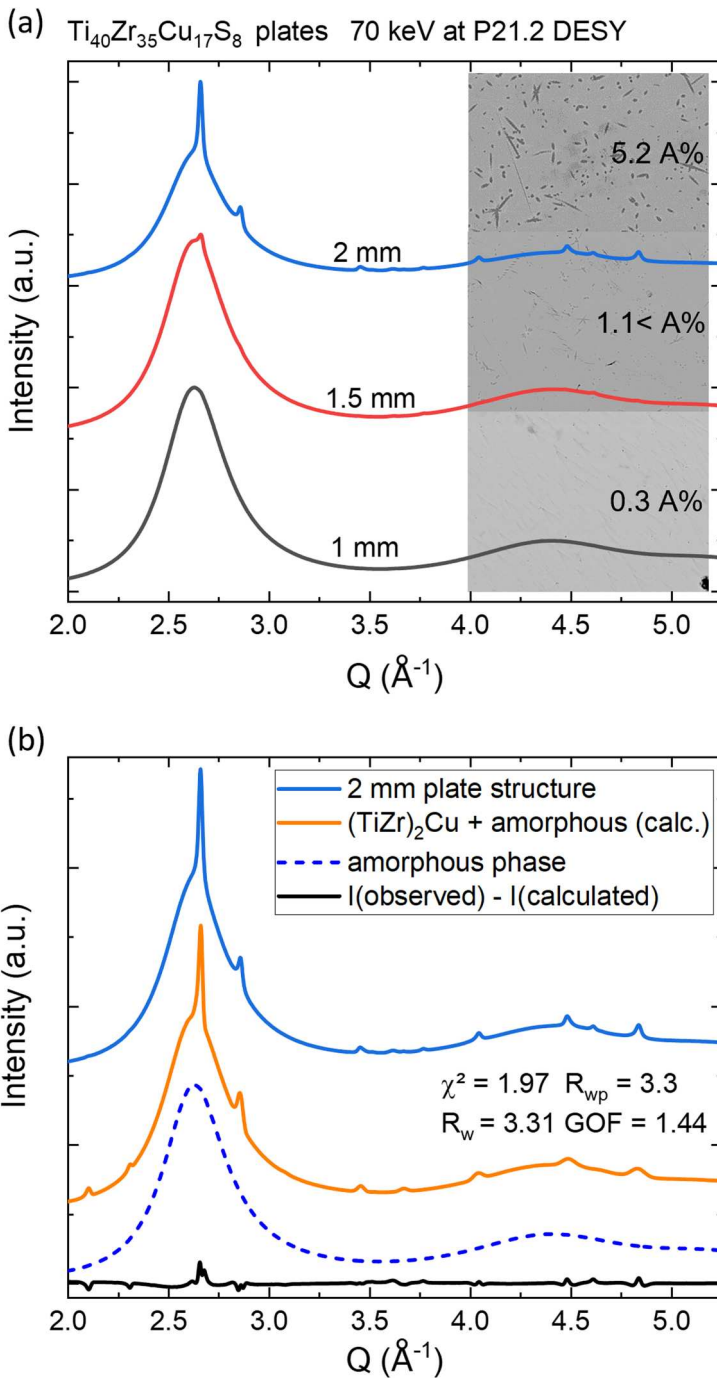


Figure 1. (a) Synchrotron diffraction data $I(Q)$ for three different plates. The insert displays the BSE contrast SEM images as well as the determined area percentage (A%) of precipitated phases. (b) Synchrotron X-ray diffraction spectra, resulting from the 2 mm thick plate of $\text{Ti}_{40}\text{Zr}_{35}\text{Cu}_{17}\text{S}_8$ (solid blue line), shown together with the theoretical spectrum (in orange), combining amorphous background (blue dashed line) and calculated intensity from the Rietveld refined $(\text{Ti}, \text{Zr})_2\text{Cu}$ cell, as well as the residual (solid black line).

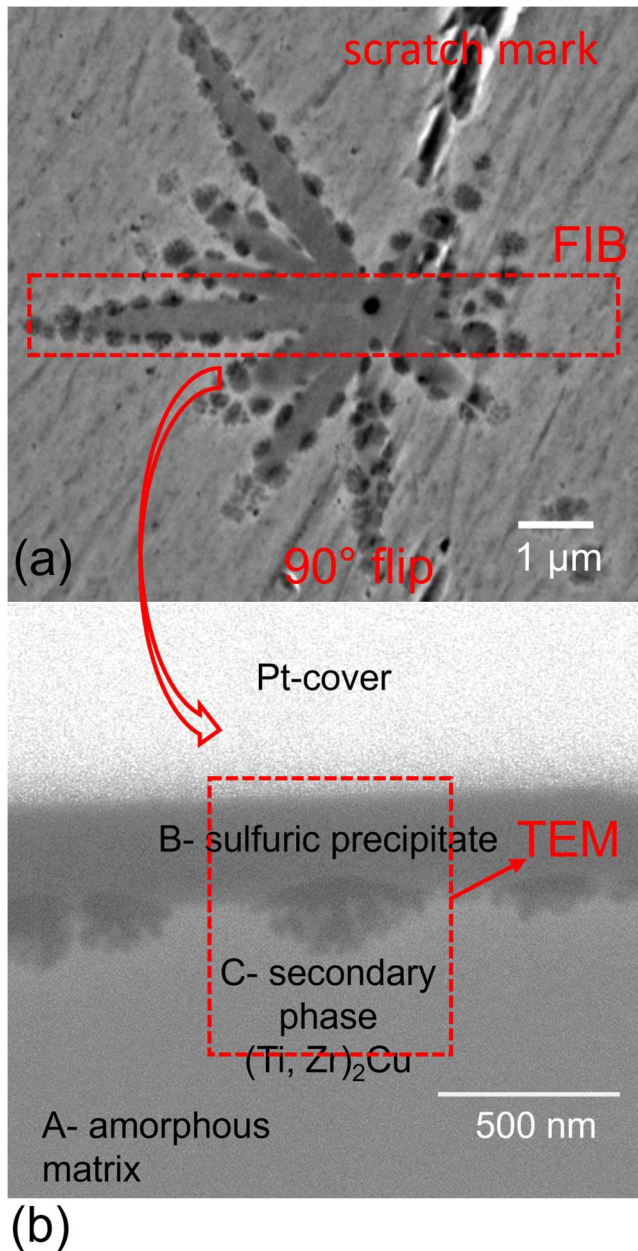


Figure 2. (a) SEM image in BSE contrasting mode showing a precipitate in the synchrotron X-ray amorphous 1.5 mm plate sample. (b) In-lens detector image, showing mainly material contrast of the FIB cut lamella with applied protective Pt-cover applied on top, for later thinning operation. The section of the sample where TEM analysis was performed on this specimen is marked by a dashed rectangle labelled TEM.

while the branches look like needles and extend from a centre. The needles correspond to the sulfuric precipitate (B) and show a decrease in copper content of 5 at%, while the sulphur content detected in the EDS rises. An overview of

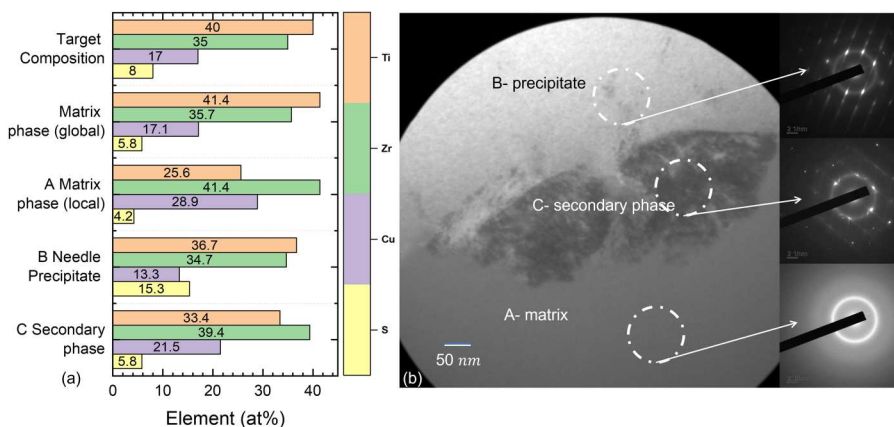


Figure 3. (a) Local TEM-EDS analysis results for the three different phases, namely the local amorphous matrix (A), the sulphuric precipitate (B) and the secondary phase (C) as well as SEM-EDS results of the global matrix phase and the nominal composition for reference. (b) TEM bright-field image of the interface between sulphuric precipitate (B) and local matrix phase (A), containing the secondary phase (C) as well as their diffraction images. The corresponding TEM-EDS spectra are shown in Figure 4.

the TEM-EDS results is given in Figure 3a. The needles contain up to 15 at.% sulphur, reflecting a significant difference in composition compared to the local matrix phase (A). In contrast, the sulphur contents in the matrix phase (A) and the secondary phase (C) are slightly reduced in comparison to the nominal $\text{Ti}_{40}\text{-Zr}_{35}\text{Cu}_{17}\text{S}_8$ composition. The local matrix phase in the area around the particles is enriched in Cu and Zr, in contrast to the global matrix phase, while the difference between the three phases (A, B and C) is more pronounced in TEM owing to the more highly localized technique. The local matrix phase shows an increase over the nominal concentration of about 12 at% for the Cu and 5% for the Zr content as well as a reduction in the Ti content.

The microstructure of the lamella in TEM bright-field imaging mode is displayed in Figure 3b, covering the exact same location that is depicted in Figure 2b and showing the local matrix phase (A), the sulphuric precipitate (B), as well as the secondary phase (C). The corresponding TEM diffraction images show significantly different scattering behaviour for the different phases. While the matrix phase displays an intense, diffuse halo pattern, both the sulphuric precipitate (B) and the secondary phase (C) show crystalline reflexes that can be distinguished as resulting from two different crystal structures. The integrated TEM diffraction image of the secondary phases (C) shares its Bragg peaks with the ones found in the synchrotron diffraction, thereby confirming that it is indeed the $(\text{Ti, Zr})_2\text{Cu}$ phase encountered in the 2 mm plate specimen. A clear identification of the sulphuric precipitate (B) turns out to be difficult, as the five observed reflections with a d-spacing value of 2.43 Å are not singular reflections but show numerous satellites, some of which are closely positioned

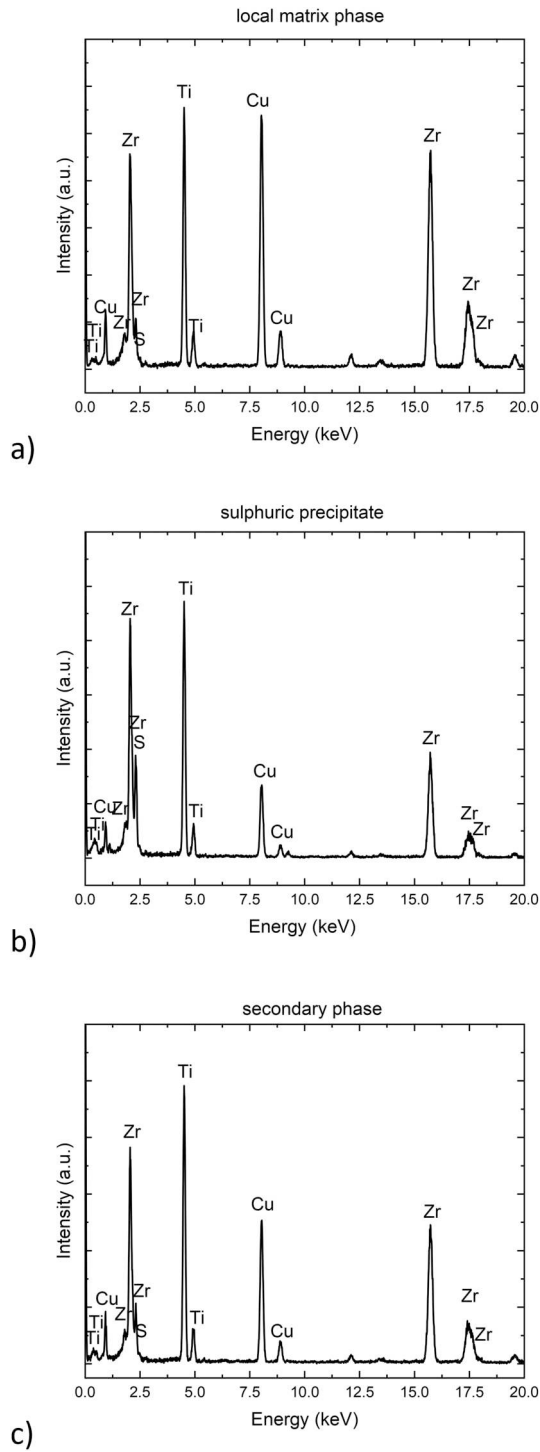


Figure 4. TEM-EDS spectra of (a) the local matrix phase, (b) the sulphuric precipitate and (c) the secondary phase.

to the main reflection, obscuring its exact maximum. Furthermore, the d-spacing matches the values of multiple possible crystallographic planes, when comparing it to the reflections listed for the reference crystal structure of Ti_8S_3 [15]. The spectrum of the latter was compared to the azimuthally integrated TEM diffraction image. The spectrum however lacks the resolution to resolve the numerous peaks of the suspected Ti_8S_3 individually. The fast-cooled nature of the sample also deviates significantly from the reference alloy that was synthesized from a Ti_2S single crystal by Owens et al. [15]. Therefore, a positive identification of the Ti_8S_3 by these methods alone is not possible, yet it appears that a similar phase has a high plausibility when considering the phase diagram of Ti-S [16] and the combined results of TEM-EDS and XRD methodologies.

4. Discussion

The $\text{Ti}_{40}\text{Zr}_{35}\text{Cu}_{17}\text{S}_8$ alloy undergoes bulk glass formation in dimensions beyond 1 mm thickness and contains neither Ni, Be nor noble metals and is therefore an interesting alloy for industrial applications. Technically the alloy produces a composite in casting thicknesses near the GFA limit. However, this has no detrimental effect if only sulphides are present. Only in higher casting thickness with significant proportions of the intermetallic compounds do the mechanical properties deteriorate. An understanding of the crystallization mechanism is crucial for further development of this system for possible applications.

Very high cooling rates are needed for S-free titanium-based Ti-Zr-Cu alloys to form glasses on account of the precipitation of crystalline phases with rather simple structures like beta titanium or binary Ti-Cu compounds [17]. Hence, the GFA is limited to thicknesses below 200 μm [9].

In contrast, bulk glass formation with critical thickness up to 3 mm is possible in the Ti-Zr-Cu-S system where the role of sulphur can be described as a kinetic retardant towards the $(\text{Ti}, \text{Zr})_2\text{Cu}$ crystal phase (C). This phase cannot form easily in the presence of sulphur owing to its poor solubility and only occurs in the locally sulphur-depleted interphase of the precipitate and the global matrix phase. The primary crystallization product after the introduction of sulphur is a complex Ti-Zr-S phase. The related sulphuric precipitates act as heterogeneous nucleation sites for the $(\text{Ti}, \text{Zr})_2\text{Cu}$ phase. To form $(\text{Ti}, \text{Zr})_2\text{Cu}$, the presence of sulphur needs to be reduced in the matrix phase. Around the sulphuric precipitates, an amorphous local matrix phase can be found which is enriched in Cu as well as Zr and depleted in S where the $(\text{Ti}, \text{Zr})_2\text{Cu}$ can form more easily.

Therefore, sulphur promotes glass formation by inhibiting $(\text{Ti}, \text{Zr})_2\text{Cu}$ crystal formation from the melt. A similar effect was observed in a previous study of our group where the retardation of icosahedral crystal phases by sulphur addition was shown, although in that case during heating from the

amorphous into the supercooled liquid region instead of cooling from the high-temperature liquid into the glass [8].

The synchrotron X-ray diffraction results only depict the secondary crystal phase $(\text{Ti, Zr})_2\text{Cu}$, even when the sulphuric precipitates are present in significant volume proportions, as in the 2 mm plate specimen which contains about 5 vol%. This arises from the large and complex unit cell of the sulphide and the fast-quenched nature of the suction cast plates, where all phases experience high cooling rates causing distortion of the unit cell. While HE-XRD is an overall robust and valuable tool for detecting even small crystalline fractions of $(\text{Ti, Zr})_2\text{Cu}$, it fails to resolve the complex and weak-scattering primary titanium-zirconium-rich sulphide phases that were found by electron microscopy.

Previously, Kuball found that the alloy's GFA of 3 mm can be produced from industrial and high-purity raw material alike, regardless of the oxygen content [10]. This robustness of the alloy's GFA and mechanical properties towards oxygen contamination is likely linked to the change in primary phase from an intermetallic compound like Ti_2Cu and Zr_2Cu . These compounds are known to primarily solidify on structurally similar oxides like $\text{Zr}_4\text{Cu}_2\text{O}$ where they can easily nucleate owing to the similar structure that reduces the mechanical properties significantly [18]. The primary sulphide crystals contained in the samples were however shown by Kuball to be not detrimental towards the GFA and mechanical properties of the alloy, even in casting thicknesses bordering the critical casting thickness of 3 mm.

5. Conclusions

In conclusion, the introduction of sulphur into the Ti-Zr-Cu system results in a change of the primary phase to a sulphide crystal phase. This phase has a high sulphur content and appears to be a complex Ti-Zr-S phase with a crystal morphology of a distinct ellipsoid shape, embedded in an amorphous matrix phase. The sulphide phase precedes the formation of the regular $(\text{Ti, Zr})_2\text{Cu}$ phase, which is usually encountered as a primary crystallization product in the system without sulphur [9] and now only encountered as the secondary phase. The initial nucleation of the $(\text{Ti, Zr})_2\text{Cu}$ phase appears to start on the interface between the sulphur-rich phase and the matrix phase. Here it is likely that the copper-enriched zones around the copper-depleted sulphuric precipitates (B) favour the local formation of the $(\text{Ti, Zr})_2\text{Cu}$ phase during the cooling and subsequent rapid solidification process.

Bulk metallic glass formation in this system depends on the sulphur addition, as no bulk glass can be formed on the titanium-rich side without it [9]. Therefore, the sulphur can be seen as a kinetic retardant towards the $(\text{Ti, Zr})_2\text{Cu}$ crystallization and hence explain the observed slowdown of crystal formation. When determining the strategies for further alloy development in this system, the sulphides play an important role and should be taken into

consideration as they hinder the formation of the regular crystalline phases that can be found in the sulphur-free variants of the $\text{Ti}_{40}\text{Zr}_{35}\text{Cu}_{17}\text{S}_8$ alloy.

Overall this combination of properties makes the alloy system pre-destined for the additive manufacturing route as the alloy possesses sufficient glass-forming ability and robustness against oxygen contamination that is within the typical oxygen contamination loads of the additive manufacturing route [19]. They will be part of further studies focussing on the additive manufacturing capabilities of titanium-based alloys containing sulphur.

Acknowledgements

We acknowledge the DESY (Hamburg, Germany), a member of the Helmholtz Association HGF and give our thanks to Dr Malte Blankenburg and Dr Ulrich Lienert for experimental support and operation of the P21.2 beamline facility during the HE-XRD experiments. The authors also thank Dr-Ing. Christoph Pauly, the Chair of Functional Materials, for preparing the lamella, and the German Research Foundation (DFG) for providing access to the Helios NanoLab600 FIB-SEM.

Disclosure statement

No potential conflict of interest was reported by the author(s).

ORCID

Bastian Adam  <http://orcid.org/0000-0001-8841-9516>

Lucas Matthias Ruschel  <http://orcid.org/0000-0001-7581-2650>

Nico Neuber  <http://orcid.org/0000-0002-9912-5764>

Maximillian Frey  <http://orcid.org/0000-0001-8602-721X>

Ralf Busch  <http://orcid.org/0000-0002-1696-271X>

References

- [1] A.I.C. Suryanarayana, *Bulk Metallic Glasses*, CRC Press, Boca Raton, 2011.
- [2] K. Han, Y. Wang, J. Qiang, H. Jiang, and L. Gu, *Low-cost Zr-based bulk metallic glasses for biomedical devices applications*. *J. Non Cryst. Solids* 520 (2019), pp. 119442.
- [3] T. Zhang, X. Meng, C. Wang, L. Li, J. Yang, W. Li, R. Li, and Y. Zhang, *Investigations of new bulk metallic glass alloys fabricated using a high-pressure die-casting method based on industrial grade Zr raw material*. *J. Alloys Compd* 792 (2019), pp. 851–859.
- [4] A. Kuball, O. Gross, B. Bochtler, and R. Busch, *Sulfur-bearing metallic glasses: A new family of bulk glass-forming alloys*. *Scr. Mater* 146 (2018, March), pp. 73–76.
- [5] A. Kuball, *Development, Characterization and Processing of a Novel Family of Bulk Metallic Glasses: Sulfur-Containing Bulk Metallic Glasses*, University of Saarland, Saarbrücken, 2019.
- [6] O. Gross, L. Ruschel, A. Kuball, B. Bochtler, B. Adam, and R. Busch, *Bulk metallic glass formation in the Ti(Zr)-Ni(Cu)-S system*. *J. Phys. Condens. Matter* 32 (2020), pp. 7.

- [7] H.-R. Jiang, J.-Y. Hu, N. Neuber, B. Bochtler, B. Adam, S.S. Riegler, M. Frey, L. Ruschel, W.-F. Lua, A.-H. Fenga, R. Busch, and J. Shen, *Effect of sulfur on the glass-forming ability, phase transformation, and thermal stability of Cu-Zr-Al bulk metallic glass*. Acta Mater. 212 (2021), pp. 116923.
- [8] L.M. Ruschel, B. Adam, O. Gross, N. Neuber, M. Frey, H.J. Wachter, and R. Busch, *Development and optimization of novel sulfur-containing Ti-based bulk metallic glasses and the correlation between primarily crystallizing phases, thermal stability and mechanical properties*. J. Alloys Compd 960 (2023), pp. 170614.
- [9] V.V. Molokanov, and V.N. Chebotnikov, *Glass forming ability, structure and properties of Ti and Zr-intermetallic compound based alloys*. Key Eng. Mater. 40–41 (1990), pp. 319–331.
- [10] A. Kuball, O. Gross, B. Bochtler, B. Adam, L. Ruschel, M. Zamanzade, and R. Busch, *Development and characterization of titanium-based bulk metallic glasses*. J. Alloys Compd 790 (2019), pp. 337–346.
- [11] B. Bochtler, *Thermophysical and Structural Investigations of a CuTi- and a Zr-Based Bulk Metallic Glass, the Influence of Minor Additions, and the Relation to Thermoplastic Forming*, University of Saarland, Saarbrücken, 2019.
- [12] B. Bochtler, J.M. Mariño-Salguero, A. Kuball, O. Gross, F. Yang, A. Meyer, O. Gross, F. Yang, A. Meyer, T. Buslaps, U. Rütt, and R. Busch, *Changes in the crystallization sequence upon sulfur addition in the bulk metallic glass-forming liquid revealed by in situ high-energy x-ray diffraction*. Phys. Rev. Mater 5 (2021), pp. 103402.
- [13] P. Juhás, T. Davis, C.L. Farrow, and S.J.L. Billinge, *PDFgetx3: A rapid and highly automatable program for processing powder diffraction data into total scattering pair distribution functions*. J. Appl. Crystallogr 46 (2013), pp. 560–566.
- [14] R. Arroyave, T.W. Eagar, and L. Kaufman, *Thermodynamic assessment of the Cu–Ti–Zr system*. J. Alloys Compd 351 (2003), pp. 158–170.
- [15] J.P. Owens, and H.F. Franzen, *Preparation and structure determination of Ti8S3*. Acta Crystallogr. Sect. B 30 (1974), pp. 427–430.
- [16] K. Hirata, S. Iikubo, H. Fujimoto, and H. Ohtani, *Thermodynamic assessment of Fe–Ti–S ternary phase diagram*. Calphad 57 (2017), pp. 62–77.
- [17] K.C.H. Kumar, I. Ansara, P. Wollants, and L. Delaey, *Thermodynamic optimisation of the Cu–Ti system*. Int. J. Mater. Res. 87 (1996), pp. 666–672.
- [18] R.D. Conner, R.E. Maire, and W.L. Johnson, *Effect of oxygen concentration upon the ductility of amorphous Zr₅₇Nb₅Al₁₀Cu_{15.4}Ni_{12.6}*. Mater. Sci. Eng. A 419 (2006), pp. 148–152.
- [19] J. Wegner, M. Frey, M. Piechotta, N. Neuber, B. Adam, S. Platt, L. Ruschel, N. Schnell, S.S. Riegler, H.-R. Jiang, G. Witt, R. Busch, and S. Kleszczynski, *Influence of powder characteristics on the structural and the mechanical properties of additively manufactured Zr-based bulk metallic glass*. Mater. Des 209 (2021), pp. 109976.